City Research Online

City St George's, University of London

Citation: Mitroglou, N. & Gavaises, M. (2013). Mapping of cavitating flow regimes in injectors for medium-/heavy-duty diesel engines. International Journal of Engine Research, 14(6), pp. 590-605. doi: 10.1177/1468087413500491

This is the accepted version of the paper.

This version of the publication may differ from the final published version. To cite this item please consult the publisher's version.

Permanent repository link: https://openaccess.city.ac.uk/id/eprint/13555/

Link to published version: https://doi.org/10.1177/1468087413500491

Copyright and Reuse: Copyright and Moral Rights remain with the author(s) and/or copyright holders. Copies of full items can be used for personal research or study, educational, or not-for-profit purposes without prior permission or charge, unless otherwise indicated, provided that the authors, title and full bibliographic details are credited, a hyperlink and/or URL is given for the original metadata page and the content is not changed in any way. For full details of reuse please refer to City Research Online policy.

City Research Online: http://openaccess.city.ac.uk/ publications@citystgeorges.ac.uk

Mapping of cavitating flow regimes in injectors for medium/heavy duty Diesel engines

N.Mitroglou and M.Gavaises

Energy and Transport Research Centre
School of Engineering and Mathematical Sciences
City University London
EC1V 0HB, UK

Abstract

Reducing the sac volume size of medium/heavy duty Diesel engine injector nozzles can minimise the fuel dripping into the combustion chamber at the end of injection events which has been linked to reduced engine-out emissions. The present study demonstrates the effect of reduction in the sac volume of Diesel fuel injectors utilised in medium/heavy duty applications on the internal nozzle flow. This is realised by comparison of two heavy duty Diesel nozzles that feature a large difference in sac volume size of almost three times. For visualisation purposes, the nozzles have been enlarged by six times and replicas were manufactured from a transparent material. High speed digital imaging was used to capture the instantaneous spatial and temporal characteristics of geometric as well as dynamic vortex cavitation structures. The investigation was conducted in a steady state flow test rig, for three different needle valve lifts. For all tested conditions, the flow behaviour was analysed at three distinct areas of the nozzle, these being the needle seat, the sac volume and the injection hole. Interpretation of experimental observations was supported by parallel computational fluid dynamics simulations of the exact conditions measured during the experiments. Post processing of the captured images has revealed the ensemble – average cavitation location, its standard deviation and the cavitation structures life – time inside the sac volume. Results showed a significant dependency of the internal nozzle flow on the sac volume size and identified clear differences in the structure of the cavitation pockets inside the sac volume under certain operating conditions.

1. Introduction

1.1 Background

The market share of Diesels has been increasing in passenger cars while it is dominant in medium and heavy duty vehicles. According to an Energy Outlook Review for 2040 **[1]**, the number of such vehicles is expected to significantly increase (more than double) over the next decades; this increase is linked with the expected construction sector in the developing countries, the continuous development or high-populated urban areas (cities) that require increased transportation of goods through trucks/trains, and the increase in the transportation of goods through ships. It is also expected that the consumption of Diesel fuel from this particular sector will double.

In general, the increasingly stringent emission legislation coupled with the need to reduce the consumption of fossil fuels is driving the development of combustion engines and their sub-systems. There are different routes to fulfil the NOx emission legislation for Diesel engines, based upon cooled Exhaust Gas Recirculation (EGR) and/or Selective Catalytic Reduction (SCR) (for example **[2]**). The Diesel Particulate Filter (DPF) strategies are being applied mainly on higher speed applications on

light duty commercial vehicles, while SCR is to be found on medium and heavy duty applications. However, in combination with EGR, the effect of injection pressure on NOx is reduced, while the effect on soot emissions is maintained. This effect has been experimentally verified by a recent study from AVL performed on a single-cylinder Diesel engine **[2]**. Modern high pressure fuel injection equipment (FIE) incorporates smaller diameter injection holes that promote atomisation and reduce PM emissions; these in turn, depend strongly on the nozzle design and in particular on the size of the nozzle sac volume. On the other hand, increased injection pressure and multiple injections make the FIE sensitive and vulnerable to cavitation erosion and damage **[3]**. An increase of injection pressure up to 3000 bar is expected to put less demand on the after-treatment systems and to result on an overall cheaper solution for the whole powertrain system. Thus, the design of durable nozzles that do not produce excessive PM emissions is of paramount importance for the next generation of Diesel FIE.

One of the well-known disadvantages of sac-type injection nozzles typically used in such applications is that fuel is trapped inside the nozzle sac volume, which is either injected at low injection pressure or is dripping into the combustion chamber following the closing of the needle valve forming a poorly atomised liquid. This undesirable and uncontrolled dripping of fuel inside the combustion chamber is one of the main drawbacks in the race for improving engine exhaust emissions. Thus, the new generation sac-type Diesel nozzles feature smaller sac volumes compared to early designs, aiming to minimise the quantity of fuel trapped and the amount of engine-out PM emissions.

1.2 Nozzle flow and cavitation phenomena

The occurrence of cavitation has been documented in the open literature since the mid ‘90s, for example see **[4-9]**. Despite the fact that only few studies have provided valuable insight on the cavitating flow in Diesel injectors (for example **[5, 8-13]**), the trend towards extremely high operating pressures and very short time scales prohibits the application of such techniques to real injectors. As a result, enlarged nozzle replicas have been utilised over the years at conditions emulating those present in production fuel systems (for example **[13-15]**). A limited number of studies have also demonstrated dynamic flow similarity based on simultaneous matching of the Reynolds and cavitation numbers. Such studies have revealed that the two-phase flow regimes realised in enlarged nozzles are directly comparable to those in real-size ones **[5, 7]**. Further supporting evidence has been provided by CFD simulations **[14]**, which have confirmed that similar flow regimes are formed despite the obvious and well known differences in the micro-scale level of bubble formation and development. Experimental data from large-scale injectors are also valuable for the development and validation of cavitation models applicable to fuel injectors. Still, up to date, no studies exist in the open literature on the prediction of vortex-type (string) cavitation inside high-pressure Diesel nozzles. This is mainly attributed to the lack of relevant experimental data for these flow phenomena, leading to an incomplete physical understanding of the process.

Investigations have demonstrated the existence of two distinct forms of cavitation inside Diesel injector nozzles **[13]**: geometric-induced and vortex or string cavitation. Geometric-induced cavitation is the most common form of cavitation and has become gradually a well-understood flow phenomenon; it initiates at the sharp corners of the hole inlet due to the abrupt acceleration of the fuel flow as it enters the nozzle holes. On the other hand, string or vortex cavitation structures have been observed in the bulk of the liquid inside sac and mini-sac type nozzles, where the relatively large nozzle volume allows the formation of large-scale vortical structures **[14, 17]**. Vortex cavitation is commonly found in propellers, hydraulic turbines and hydrofoils as described in **[18-21]** which can cause erosion and become the source of several undesirable effects such as a sharp reduction in performance and increased noise and vibrations **[3, 22]**. Recent studies have confirmed similar behaviour in multi-hole nozzles for high-pressure direct-injection gasoline and Diesel engines **[15, 23, 24]** which is generally accepted as promoting fuel atomisation. In a previous study by the authors' group, it has been established that cavitation strings mainly represent a transport mechanism of the vapour to the core of recirculation zones. These recirculations can develop at pressures much higher than the fluid vapour pressure and so there is no phase-change (cavitation) process of the fuel itself. The studies of **[10, 15, 23, 24]** have indicated that cavitation may be also associated with hole-to-hole and cycle-to-cycle variations that can make a contribution to higher engine-out emissions **[3]**. Moreover, recent studies **[10, 17]** have provided evidence that geometric-induced and vortex cavitation structures can interact, thus increasing the inherent instability of such transient flow fields.

1.3 Present contribution

The latest developments in Diesel fuel injection equipment involve reduction in the sac volume of nozzles while at the same time keeping unchanged some important design characteristics that affect fuel delivery such as the needle valve shape, hole size and orientation. Still, very little is known on the effects of such geometric changes to the detailed cavitating flow patterns formed within the nozzle sac volume. The present study aims to address the differences in internal nozzle flow associated with the sac volume size using a combined experimental and computational approach. Two typical nozzle geometries, characteristic of such Diesel engine applications have been utilised. Experimental investigations include high-speed imaging of the sac volume and injection holes flow for two large-scale, transparent, sac-type nozzle replicas. Detailed observations reveal that small-size sac volume nozzles are more prone to string/vortex cavitation formation than larger nozzle designs to a degree that, to the best of our knowledge, *has not been reported before*. In particular, it has been observed that intense vortical structures can induce cavitation formation inside the bulk flow of the liquid as opposed to the vapour transport observed in the past. Use of CFD simulations has provided information on the local flow field at the locations where string cavitation develops, thus contributing to a more detailed interpretation of the experimentally acquired data. Post processing of images obtained over a long period of time under well-defined and controlled conditions reveal the lifetime of

the string cavitation structures inside the sac volume. In the following sections of the paper, a brief description of the experimental apparatus is given together with the nozzle designs and operating conditions tested. A brief summary of the simulation tool employed is also provided. Then, the findings of this investigation are analysed in the results section, followed by a summary of the most important conclusions.

2. Experimental set-up, simulation model and test cases

Cavitation visualisation data presented in the following sections have been obtained in two enlarged (by a factor of six) transparent nozzle replicas. The model nozzles were manufactured from a clear, acrylic material (Perspex) and have five cylindrical injection holes. Both designs feature sharp entry injection holes of 2.1×10^{-3}m diameter, their hole length over diameter ratio is fixed at L/D = 3.75 and the maximum needle valve travel is 1.87×10^{-3}m. Given the enlargement factor of 6, the corresponding real-size dimensions are 350×10^{-6} m and 312×10^{-6} m for the hole diameter and full needle valve lift, respectively. Based on the above design constraints, the enlarged models of both nozzles feature a total injection hole volume of 156.8×10^{-9} m^3. Additionally, both nozzles share an identical needle seat diameter. Figure 1(a, b) illustrates a section of the two 5-hole nozzles; the main differences in these designs are the morphology of the nozzle downstream the needle seat and the sac volume size. The first nozzle, referred to as "large sac volume" (Figure 1a), features a sac volume of 1035×10^{-9} m^3 volume, which is almost 6.6 times larger than the corresponding total injection holes volume. The second nozzle, presented in Figure 1b, features a sac volume size of almost one third of the first model (340×10^{-9} m^3) and is thereafter referred to as "small sac volume" model. An appreciation of the size of the sac volume for both nozzles is obtained if it is compared against the injection quantity of a nominal injection event of 1ms duration at 2000 bar injection pressure. Using the measured values of the nozzle discharge coefficient as shown in the following section, it can be estimated that the small sac nozzle features a volume of ~1.6% of the total injected quantity of a typical main injection event while the same value for the large sac volume nozzle is ~3.2%. This number represents more than 50% for short pilot or post injection events and thus it is clear that it can be a major contributor to engine-out emissions.

The visualisation studies reported in the following sections provide observations and statistical analysis of the flow characteristics in these two aforementioned nozzles. High-speed images have been collected at fixed needle lift positions at various combinations of injection and back pressures. The steady-state flow rig that has been described in detail in past studies **[16]** has been utilised. The working fluid was filtered water kept at a constant, controlled temperature of 25°C. Flow rate through the model was controlled by a valve downstream the feed pump and monitored by an ultrasound flow meter. The pressure difference across the model was controlled by adjustment of the inflow and outflow of the injector through appropriate flow valves. Enhancement of the cavitating flow

conditions through the nozzle was realised with the use of a suction pump, installed alongside the main feed pump. Pressure was monitored at two locations, upstream the needle valve seat and downstream of the injection hole exit, right at the expansion hole of the collector; this has allowed accurate calculation of the discharge coefficient of the two nozzles.

The operating conditions and the individual nozzle characteristics for both large-scale models are summarised in Table 1. Results are presented at 20×10^{-6}m, 50×10^{-6}m and 312×10^{-6}m (full needle lift) equivalent real size needle valve lifts. For both nozzle designs and needle lift values, a low and a high CN condition are presented, as summarised in Table 1. The cavitation number (CN) is defined as $CN=(P_{inj}-P_{back}) / (P_{back}-P_V)$, where P_{inj}, P_{back}, and P_V represent the injection, downstream liquid (injection into liquid), and fluid vapour pressures, respectively. During engine operation this number varies typically between 1 – ~30 depending on the pressure inside the nozzle sac volume and combustion chamber pressure at the time of injection; in the presented cases, cavitation numbers tested varied from 5 to 21, which correspond to large-scale model injection and downstream pressure variations of 5-15 bar and 0.7-1 bar, respectively. The equivalent injection pressure that corresponds to the high CN value is ~1800 bar assuming injection close to TDC of a turbocharged Diesel engine. The Reynolds number, *Re,* is defined on the basis of hole diameter and mean injection velocity; the values tested here are in the range of 10,000 to 53,000 which are typical for such injection nozzles.

As cavitation structures behave transiently within very short time scales even under steady-state conditions, a high-speed camera system was used, which is able of acquiring 20,000 frames per second at sub-μs shutter speeds. In total, 10,000 images were collected for each test case; both side and bottom view images have been obtained simultaneously. To eliminate any source of background light being scattered on the camera, a series of background images have been acquired at minimum flow rates through the nozzle, which could capture any shadows in the acquired images that are not connected to cavitation. This series of background images are then subtracted from the data images and a mask is applied isolating the imaged sac volume region from the needle seat and injection holes. Following the isolation of the region of interest, a light intensity identification technique was applied in order to identify the boundaries of the cavitation structures. An optimum threshold value was selected and applied to all acquired images. The threshold images were converted to binary images; a value of 1 was assigned to the cavitating areas and 0 to the non-cavitation areas. Superposition of all acquired images results to an estimation of the mean cavitation image and its standard deviation; these can be interpreted as probability density functions of the vapour existing inside the sac volume. Finally, the frequency of appearance of the cavitation strings over the complete acquisition duration has been recorded.

In the absence of quantitative flow measurements inside the nozzle sac volume and injection holes, the use of CFD was considered essential for assisting in the interpretation of the acquired images. The

GFS CFD code has been used **[25]** with its cavitation model been validated against a number of experimental data available for both single-phase and two-phase cavitating nozzles; thus details of the model are not repeated here. The computational domain is created using a CFD pre-processor (ANSA), which has the specific capability of reproducing the complete domain with hexahedral cells. Following several sensitivity analyses in terms of the cell numbers simulated, it has been found that the code is rather insensitive to the grid density when approximately 500k hexahedral cells are selected. The measured pressures upstream and downstream of the nozzle have been assigned as fixed pressure boundary conditions at the inlet and exit boundaries, respectively. Only one sector of 1/5 of the whole nozzle has been simulated assuming symmetric boundary conditions. As the purpose of the present paper is not to perform a detailed CFD study but rather assist in the interpretation of the experimental results, the flow has been assumed to be steady-state and single-phase in the simulations performed. The Realisable k-e model of turbulence **[26]** with enhanced wall functions **[27]** has been employed in these calculations.

3. Results and discussion

In this section the various results obtained are presented and discussed. Prior to the detailed presentation of the observed flow characteristics, the measured discharge coefficient values for both nozzles and needle valve lifts are illustrated in Figure 2. The highest discharge coefficient presented in the graph is 0.61 and it corresponds to the large sac volume nozzle operating at full lift and low CN. The measured maximum value is considerably low and this is mainly attributed to the sharp injection hole inlet corners that promote geometric-induced cavitation, combined with the parallel hole shape of the model representing the cylindrical injection holes. As reported in previous studies **[14]**, based on CFD predictions of cavitation using the model presented in **[25]**, cavitation may be responsible for up to 15% reduction in the nozzle discharge coefficient at low needle lifts, with its relative significance increasing with the extend of cavitation. Additionally, at low needle lift conditions, it is evident from the graph in Figure 2 that between low and high CN conditions the discharge coefficient remains almost at identical levels, which implies that the main throttling of the nozzle takes place at the needle seat area. However, the corresponding values for the full lift cases exhibit differences in the measured CN.

Comparison of the values presented in Figure 2 between the two nozzles reveals a significant reduction in the discharge coefficient as the sac volume size decreases, for all investigated needle lift conditions. In particular, at low needle lifts the small sac volume nozzle features more than 50% reduction in the discharge coefficient compared to the large sac volume case. As the needle lift increases to its maximum setting, the difference in the measured discharge coefficient between the two nozzles decreases to almost 20%, whereas the small sac volume nozzle hardly reaches values of 0.5. Based on the injection hole shape and design features of both nozzles, such a variation in the

discharge coefficient is not anticipated; thus, further insight on the phenomena is provided by high-speed imaging of the flow inside both nozzles.

3.1 20μm Real-size Equivalent Needle Valve Lift

The minimum possible needle valve lift setting was selected to be 20×10^{-6} m equivalent lift of the real-size nozzle, which corresponds to 0.12×10^{-3} m for both large-scale nozzles. At such extra low values of needle valve lift, needle seat cavitation exhibits intensity values that depend strongly on the design characteristics of the seat area. The design of the needle seat area differs considerably between the two investigated models; the large sac volume nozzle features a short-length seat area followed by a short-length diffusion zone upstream of the sac volume. On the contrary, the small sac volume design exhibits an elongated diffuser-like feature that has a significantly low divergence in annulus channel width. The differences in needle seat design between the two nozzles are explained in detail in the previous experimental set-up section (Section 2).

As illustrated in Figure 3, the large sac volume nozzle exhibits a significant pressure drop right after the seat neck region that is introduced by an abrupt acceleration of the flow. On the other hand, the shape of the channel annulus downstream the needle seat area in the small sac volume nozzle gently accelerates the fluid flow, and maximum velocities, i.e. lowest pressure in the region, are reached at the entry of the sac volume. Thus, this design did not produce needle seat cavitation during all investigated conditions; instead, cavitation was experimentally observed at the entry of the sac volume and it is in full agreement to the predicted pressure distribution.

The large sac volume nozzle showed consistent needle seat cavitation structures that dominated the needle seat region at very low needle valve lifts (Figure 4), regardless of the cavitation number setting. The probability of vapour pockets to appear at the needle seat region is high and, as denoted by the mean image in Figure 4b, the cavitating structures reach and even exceed 50% of the measurement period. Additionally, as illustrated in the standard deviation image (Figure 4c) the phenomenon is fairly stable as standard deviation values hardly exceed 7%. On the contrary, the small sac volume nozzle design, as highlighted previously, does not present any signs of needle seat cavitation. Instead, the predicted pressure drop at the sac volume entry, at pressures below the liquid vapour pressure, was verified in the form of intense and highly unstable cavitation pockets observed inside the sac entry region. As illustrated in Figure 5, cavitation occurred at the sac entry region at random spatial locations around the periphery of the sac. The nature of these structures is found to be unstable in shape and highly transient, as opposed to the structures observed in the large sac volume nozzle. Although the recorded behaviour is not classified as needle seat cavitation, it is only observed at very low needle valve lifts. Moreover, as extremely low needle valve lifts magnify the effect of the random eccentricity between the needle valve and the injector body, repeatability studies have confirmed the aforementioned behaviour for both nozzle designs.

The appearance of cavitation at the needle seat area creates potential nucleation sites that are convected downstream inside the sac volume and induce further structures that, in some cases, are capable of completely altering the flow inside the nozzles. At very low needle valve lifts, it has been verified that the design of the seat area affects the appearance of cavitation inside the sac volume. In the large sac volume nozzle, the observed needle seat cavitation has not proven strong enough to induce further flow disturbances inside the sac volume. In particular, vapour pockets that have been previously generated at the needle seat region, are transported inside the sac volume. The observed structures, combined with the high pressure levels in the sac (Figure 6), collapse as they enter the sac volume, without creating any disturbance to the flow field. Investigations showed that the lifetime of such structures is very short and of the order of $50 - 100 \times 10^{-6}$s. For a measurement period of 0.5s, the probability of appearance was found to be negligible. Furthermore, the low flow velocities inside the large sac volume nozzle at this extra low needle lift produced weak recirculation zones that proved unable to promote string cavitation; it was only visible for less than 1% of the total acquisition period.

The small sac volume nozzle, however, showed different behaviour than the large sac nozzle under the same operating conditions. Initially, it has been confirmed that cavitation pockets created at the sac entry, due to the needle seat design, do influence the sac flow considerably. As illustrated in Figure 6, the structures observed inside the sac volume are relevant to the ones presented in Figure 5 and mainly exist around the periphery of the sac. These structures cannot be classified as cavitation strings, as reported in several previous studies (selectively **[17]**), but rather as vapour pockets that, following their appearance at the sac entry, grow further. Cavitation strings have a shape of well-defined vapour tubes. As suggested in **[14, 17]**, cavitation strings can appear in locations where surrounding pressures are typically much higher than the fluid's vapour pressure and represent transport of vapour rather than fluid nucleation in these locations. On the contrary, the observed vapour structures in Figure 5 do represent formation of cavitation at these locations, which is supported by the predicted pressure field inside the small sac volume (Figure 6) where pressures below vapour pressure were calculated. Moreover, streamlines illustrated in Figure 6 clearly demonstrate the tendency of the small sac volume to form flow recirculation zones in a confined volume of much smaller size compared to the large sac volume nozzle. Therefore, combination of flow recirculation with pressure values at the core that are well below the vapour pressure of the liquid can cause extensive formation of vapour pockets inside the sac volume.

The observed flow field tends to have a chaotic behaviour at this extra low needle lift; vapour structures seen to occupy a large fraction of the nozzle's sac volume depending on the pressure difference across the nozzle. As illustrated in Figure 7, at low cavitation numbers the mean projected area of the sac volume occupied by cavitation clouds is relatively small; however, the topology and shape of the vapour pockets are random and highly unstable, as the large values of standard deviation indicate. An increase in the cavitation number leads to the sac volume of the nozzle being occupied by

a large vapour cloud. The average projected area covered by cavitation structures can be as large as 70% of the total projection area; significant instabilities in terms of the spatial location have been recorded, as shown in the standard deviation images of the high CN case. This chaotic flow behaviour of the small sac volume nozzle has an immediate effect on the nozzle discharge coefficient (Figure 2) as at an equivalent real-size lift of 20×10^{-6} m, the measured discharge coefficient is found to be just 0.13 which is extremely low even for very low needle valve lifts.

It has been established in previous studies that the flow development inside the sac volume is responsible for the inherent instabilities in the injection hole flow field. A direct comparison of the flow structures inside the injection holes of both nozzles, at the extra low needle lift (20×10^{-6} m equivalent real-size lift), showed that the sac volume flow is responsible for the shaping of the flow inside the injection holes. As illustrated in Figure 8, the large sac volume nozzle exhibits an unexpected behaviour of the liquid inside the injection hole; although geometric cavitation forms at the sharp hole inlet, the vapour structures extend only a small distance inside the hole, as the presented data refer to a low cavitation number of 7. According to the results presented in previous sections, at extra low needle valve lifts the large sac volume nozzle features needle seat cavitation that is unable to alter the sac flow significantly due to low flow rates through the nozzle. Therefore, the flow inside the sac is considered stable with a negligible presence of cavitation strings. On the contrary, the small sac volume nozzle, illustrated at the right-hand side of Figure 8, showed as expected different hole flow structures. At a cavitation number of 7 and extra low needle valve lift, the flow through the injection hole is highly unstable and heavily influenced by the sac volume flow field. At such conditions, this nozzle was found to have the majority of its sac occupied by unstable vapour pockets that are then convected towards the injection hole. The aforementioned instability, coupled with the calculated low flow velocities inside the hole that are about a third of those in the large sac volume case (Re = 12,000), cause a delay in the appearance of geometric cavitation. Instead, vapour pockets generated inside the sac volume are finding their way through the holes inducing significant instabilities.

3.2 50µm Real-size Equivalent Needle Valve Lift

The highly transient internal nozzle flow behaviour imposed by the movement of the needle valve exhibits increased instabilities particularly at the early stages of needle movement. Thus, following the extra low needle valve lift of 0.12×10^{-3} m (20×10^{-6} m real-size equivalent), attention is also focused on 0.3×10^{-3} m (50×10^{-6} m real-size equivalent), a setting that represents almost 16% of full lift; this is still a low needle lift setting, which marks the transition from a highly unstable internal nozzle flow structure to a more stable behaviour that is closer to full lift conditions for the two investigated nozzles.

As the needle valve approaches the upper limits of the “low lift” region, needle seat cavitation diminishes in the large sac volume nozzle case, as expected. Similarly, in the small sac volume nozzle, the effect of vapour generation at the sac entry due to the increased velocities associated with extra low needle valve lifts is minimised. This is expected to alter the behaviour of the flow inside the sac volume of both nozzles. CFD predictions of the pressure distribution as well as flow streamlines are presented for both nozzles in Figure 9. For both designs, the flow is attached to the needle valve surface, as it enters the sac volume at low needle lifts; this spatial flow arrangement gives rise to formation of two main recirculation zones, at both sides of the injection hole. The pressure level (Figure 9) inside the core of the recirculation zones is lower compared to the rest of the sac volume; however, in the small sac volume nozzle the pressure levels are close to the vapour pressure of the liquid. Furthermore, the sac inlet stream velocity values, as predicted from the flow simulations, indicate that the liquid enters the small volume sac with up to 50% higher velocity compared to the large sac volume nozzle. Overall, the observed behaviour is expected since a similar amount of liquid (for both nozzles) is found to recirculate in the much smaller volume leading to much higher stream velocities and thus, the formation of cavitation. Experimental verification of the above findings is provided in Figure 9.

Following the improved understanding of the sac flow differences between the two nozzles at low needle lifts, it is rendered essential to quantitatively characterise both nozzles in terms of string cavitation inside the sac volume at low lift conditions. String cavitation analysis at lower needle lifts has confirmed the transient and unstable behaviour observed in past investigations. Although previous experimental results concentrated on transient injection events featuring a complete profile of needle opening and closing phases, results in the current steady-state experimental investigation have confirmed that at low needle valve lifts the observed phenomena inside injector nozzles are as transient as in real injection events. However, the time scales of the associated cavitation structures and their residence times are much longer compared to the actual injection events. Furthermore, the capability provided by the steady-state flow rig to investigate a wide range of cavitation numbers, as opposed to the narrow operating window of a real injector, allows useful observations of the effect of the flow, through the nozzle, on string cavitation to be made.

Figure 10 illustrates sac volume cavitation mean and standard deviation images over the 0.5s acquisition time for the large sac volume nozzle and two cavitation numbers. Overall, the probability of appearance of string cavitation inside the sac is relatively low, at around 8%, for both investigated cavitation numbers. Standard deviation images reveal the transient nature of the flow field, although absolute numbers are found to be smaller, compared to the previously presented cases. However, the observed spatial deviation of the cavitation structures denotes that at low needle lifts the flow field appears to be unstable. An interesting finding associated with the large sac volume nozzle is in connection to the string cavitation preference in terms of hole numbers. At low cavitation numbers,

string cavitation is found to connect mainly two sets of injection holes; however, as illustrated in the corresponding high CN case of Figure 10, this preference switches to another set of injection holes. Nevertheless, the needle valve concentric position is guided with a tolerance of 3×10^{-6}m in diameter for the six times (×6) enlarged model, ruling out any source of potential eccentricity. Finally, the frequency of appearance of these structures at both conditions of low and high CN and at low needle lifts, in the large sac volume nozzle case, is presented in Figure 11. Residence time refers to the average lifetime of single string structures asocciated with corresponding hole numbers; the delay time denotes the average time between disappearance of one string and appearance of the next at the same location (hole number). All presented values are expressed in ms for a total measurement period of 0.5 s. Residence and delay times of appearance of string cavitation are comparable in the two cases. The highly transient nature of the phenomena is graphically represented in Figure 11 by means of the standard deviation of the delay time that is plotted as error bars on the delay times bar chart; in most of the injection holes, the standard deviation could be as high as 50% of the measured delay time.

An identical investigation has been conducted for the small sac volume nozzle and at low needle lifts which revealed remarkable results regarding the type of cavitation structures recorded, rather than the variability and frequency of the string appearance. As illustrated in Figure 12, the observed structures do not classify as cavitation strings and, according to the CFD analysis, there are strong vortical structures inside the sac volume. The mechanism of creation of such vapour pockets inside the sac volume is attributed to the calculated high stream velocities coupled with the small sac volume that causes extensive pressure drop in the core of the recirculation zones and promotes locally cavitation. However, the highly transient nature of the flow inside the sac is deforming these recirculation zones rapidly and randomly. As a result, the low pressure regions extend beyond the strict core definition of the vortices, creating the observed vapour pockets. It is expected that as several nuclei exist inside the sac at these flow conditions, the injection hole flow is also affected in terms of cavitation inception and stability, resulting in a low nozzle discharge coefficient as already stated earlier. It is thus evident that the observed structures do not classify themselves as strings in the following analysis, but rather treated as cavitation pockets/clouds.

As Figure 12 illustrates, the pattern the cavitation clouds create inside the small sac volume does not change with cavitation number at low needle valve lifts. The mean images reveal an extremely high probability of cavitation appearance in the small sac volume nozzle. All nozzle holes are engaged in this phenomenon and the vapour pockets topology seems to create a coronary shape inside the sac. The small sac volume nozzle features an overall sac height almost half that of the large sac nozzle, that results in the needle tip to be at a level that partly covers the injection holes at low lifts. This geometric feature reduces even further the sac volume available to the flow and forces the recirculation zones to occupy the sac periphery around the needle tip. Following the increased probability of vapour appearance inside the small sac nozzle, the standard deviation images reveal that

almost all of the projection area of the sac is highly unstable featuring large standard deviation values. This instability is identifiable as recirculation zones inside the sac do not cavitate all around the sac periphery simultaneously; instead, cavitation vapour appears in patches at random angular locations around the periphery. It is clear from the observed structures that strings do not exist and cavitation vapour pockets cannot be linked to certain injection holes, in the case of the small volume nozzle; therefore, residence times are not presented similarly to the previously reported analysis. Overall, it is in the small sac volume nozzle that there is evidence of enlarged sac cavitation structures, compared to the large sac volume one. The identified difference between large and small sac volume flow conditions, in terms of string/cavitation structures appears to be larger than expected.

The associated injection hole flow at the low valve lift of $0.3\times^{10-}3$ m has also been investigated and found to follow the pattern identified in the case of the extra low needle valve lift. Figure 13 illustrates cavitation structures observed inside the injection holes for both nozzles at 50×10^{-6} m equivalent real-size lift and for two cavitation numbers. In the case of low CN, incipient geometric cavitation structures have been identified at the top and bottom sides of the hole inlet for the large sac volume nozzle, exhibiting a rather transient behaviour. As cavitation number increases with the needle fixed at low lifts, vortical string structures appear in conjunction with geometric cavitation clouds to form a highly transient flow field inside the injection hole of the large sac volume nozzle. On the other hand, the small sac volume nozzle exhibited an interactive flow between string and geometric cavitation regimes, characterised by a highly transient nature. At low needle lifts and at both low and high CN cases the observed flow field is unstable, featuring strong interactions between geometric cavitation and the intense vortical structures that coexist. The identified mechanism suggests that cavitation bubbles formed at locations where geometric cavitation already exists, are trapped inside the low pressure core of these vortices forming cavitation strings that extend beyond the injection hole into the sac volume.

3.3 Full Needle Valve Lift

The flow field inside both nozzles varies significantly as the needle lift increases. At full needle lift position, the sac volume inlet velocity stream now follows the sac volume wall profile, as opposed to the low needle lift cases where the flow was attached to the needle surface. Based on the simulation results, the calculated velocity variations inside the small sac volume nozzle create an unstable flow field that is more likely to be prone to string cavitation formation. This has been verified by experimental investigations that confirmed increased probability of string appearance for the small sac volume nozzle. Figure 14 illustrates the mean and standard deviation images of the sac volume bottom-view, for the two nozzles and at full needle lift conditions. The presented results refer to the highest cavitation number tested since it exhibited almost identical behaviour to the low CN test case. The mean and standard deviation images presented in Figure 14 represent the whole measurement duration of 0.5s. The maximum probability of string appearance at these conditions belongs to the

small sac volume nozzle and it is of the order of 12%, during the 0.5s period. The latter is expected, as indicated earlier, due to higher velocity recirculation zones inside the sac, compared to the large sac volume nozzle.

The large sac volume nozzle presented an extremely low probability of string cavitation formation (~3%) and the sac volume flow field appeared to have lower instabilities, compared to the small sac volume one, as it is depicted from the calculated standard deviation profile. In addition to the spatial investigations presented, Figure 15 illustrates the temporal behaviour of string cavitation inside the two nozzles. During the measurement period of 0.5s, average string cavitation residence times have been recorded and presented per injection hole, along with the average delay in occurrence of the next string cavitation at the same location. The first important observation concerns the average residence times of strings inside both nozzles. Vortical structures that form streams of bubbles appear to have an average lifetime inside both nozzles of just below 1ms. The main difference recorded, in terms of the sac volume size, is the delay time until the next string cavitation structure appears. Effectively, this number denotes the frequency at which strings appear inside the two nozzles. This frequency is measured to be greater for the small sac volume nozzle at all presented delay times except for hole number three, where it is shorter than the corresponding one of the large sac volume nozzle. Furthermore, an important feature illustrated in the temporal plots (Figure 15) is the standard deviation of the measured residence and delay times, presented as error bars on top of the data bars. The error bars denote the very small variability in the measured residence times, unlike the delay times that show extremely large variability, demonstrating the highly transient nature of the observed flow characteristics.

The predicted flow variations inside the sac volume of both nozzles inevitably affect the flow inside the injection hole and, subsequently, the emerging spray quality and stability **[23]**. At the full needle valve lift position, the flow field inside the injection holes of both nozzle designs is illustrated in Figure 16. On the left-hand-side column of Figure 16, the large sac volume nozzle features a fully developed cavitating flow for a range of operating conditions up to CN = 17 and full needle lift. Geometric cavitation seems to exist all around the sharp hole entry and extends to some length inside the injection hole depending on the flow characteristics. The flow is fully detached from the hole wall and forms a well-defined cavitation pocket, as described in previous studies **[13]**, that is similar to an open or closed horse-shoe configuration initiating around the hole entry. The observed flow field for the large sac volume nozzle is stable and the observed cavitation regimes do not show any significant changes throughout the 10,000 images acquired at 20,000 frames per second under steady state flow conditions. However, the same statement is not true for the small sac volume nozzle, presented on the right-hand-side column of Figure 16. Under all investigated conditions at full needle lift, the small sac volume nozzle exhibited a significantly different behaviour to the one described above. Geometric cavitation structures do not seem to occupy the injection hole but rather exist at confined spaces at the

top and bottom hole entry sites. The main feature that dominates the flow through the injection hole is string cavitation. The observed vortical structures appear to always extend inside the sac volume and to either link adjacent holes or attach to the needle surface. Furthermore, the part of the vortices that enter the injection hole seem to form hollow cone structures, increasing in diameter as they progress towards the hole exit. These intense vortices seem to trap cavitation bubbles at the core, becoming visible to the camera. The observed expansion in their diameter as they enter the injection hole, is abrupt and blocks geometric cavitation structures from developing further to form vapour pockets, as the flow through the hole is significantly throttled. The observed phenomenon results in partially blocked injection holes leading to relatively low discharge coefficients of the order of 0.5. Moreover, the exhibited behaviour of string cavitation inside the holes of the small sac volume nozzle is of a highly transient nature. The observed differences regarding the flow inside the injection hole between the two nozzle designs and its transient behaviour are mainly attributed to the difference in the sac volume size.

4. Conclusions

The present study has focused on assessing the flow field of two enlarged Diesel nozzles, featuring two different sac volume sizes. The specific designs tested included two large-scale (times six scale factor) five-hole nozzles with identical cylindrical injection holes but different sac volume sizes; the second nozzle was almost one third of the corresponding first nozzle sac volume. Data have been acquired for three needle valve lift settings. The investigation covers a wide range of operating conditions and it demonstrates a flow map ranging from low to full needle valve lifts. A combination of experiments and computational fluid dynamics predictions has been used in an attempt to formulate a link between the sac volume size and transient cavitation structures. Images have also revealed the formation of needle seat cavitation for the large sac volume nozzle, at the lowest needle valve lift tested. Corresponding structures were not observed at the needle seat area for the small sac volume nozzle; on the contrary, the maximum pressure drop was recorded further downstream at the entrance of the sac. Combination of images and flow predictions have revealed the global characteristics of the flow inside high-pressure nozzles that dictate the flow that follows the needle surface as it enters the sac at low needle lifts, while it gradually detaches from the needle and steers towards the sac wall as lift increases. Moreover, the flow inside the sac proved to be highly unstable at low lifts, particularly for the small sac nozzle; this is mainly attributed to the fact that a similar amount of liquid for both nozzles is forced to recirculate inside a confined volume (almost three times smaller than the large sac nozzle), thus generating high vorticity that leads to pressure drop below the vapour pressure of the liquid. The resulting cavitation structures were highly unstable and found to occupy a large percentage of the sac volume projection area. An increase in needle valve lifts caused the sac pressure to rise; however, string cavitation was recorded and its frequency of appearance was linked to the remaining

flow recirculation zones formed inside the small sac nozzle. Furthermore, at full needle valve lift, the small sac volume nozzle maintained the observed flow instabilities inside the sac that were in turn convected to the injection hole flow, inducing dynamic cavitation structures. Similar behaviour was not recorded for the large sac volume nozzle, as at full needle valve lift the flow through the injection hole was fully developed and partially detached from the hole wall; the appearance of string cavitation was at a minimum due to the weak vortex structures developed.

The combination of experimental and computational investigations has also assisted in the understanding of the unusually low discharge coefficients measured. The sharp hole inlet shape was found to promote geometric-induced cavitation and to limit the maximum discharge coefficients measured; however, the small sac volume nozzle demonstrated a discharge coefficient consistently lower than the large sac volume nozzle. This is attributed to the flow behaviour inside the sac volume that promotes intense recirculation zones; at low lifts these vortices generate vapour at their core, due to low local pressures, and as lift increases these vortices are fed into the injection hole where they promote an increase in vapour fraction, effectively throttling the nozzle. Finally, it can be argued that small sac volumes are offering advantages due to reduced dripping inside the combustion chamber after an injection event as is generally accepted but the present study indicates that the design of a high performance nozzle with a small sac volume and stable/repeatable emerging sprays remains a challenge. The aim should be to combine the advantages of small nozzle sac volume in terms of reduced dripping with the spray stability achieved with larger sac volumes.

5. Acknowledgements

The authors would like to express their gratitude to BETA-CAE Systems S.A. for providing their powerful pre- (ANSA) and post- (μETA) processing solutions for the computational fluid dynamic studies included in this investigation.

References

1 **ExxonMobil.** The Outlook for Energy: A View to 2040, 2012 .

2 **Daum S, Gill D, and Theissl H.** Medium and heavy duty diesel fuel injection system requirements to meet future emissions legislation. *IMechE Conference on Fuel Injection Systems for IC Engines, London*, 2012 .

3 **Gavaises, M.** Flow in valve covered orifice nozzles with cylindrical and tapered holes and link to cavitation erosion and engine exhaust emissions. *International Journal of Engine Research*, 2008, **9**, 435-447.

4 **Soteriou, C., M. Smith, and R. J. Andrews.** Cavitation Hydraulic Flip and Atomization in Direct Injection Diesel Sprays, *IMechE Conference on Fuel Injection Systems for IC Engines, London* , 1993 .

5 **Arcoumanis, C., M. Badami, H. Flora, and M. Gavaises.** Cavitation in Real-Size Multi-Hole Diesel Injector Nozzles. *SAE Technical Paper 2000-01-1249* , 2000

6 **Nishida, K., S. Ceccio, D. N. Assanis, N. Tamaki, and H. Hiroyasu.** Characterization of Cavitation Flow in a Simple Hole Nozzle. *International Journal of Fluid Mechanics Research*, 1997, **24,** 370-379

7 **Soteriou, C., M. Smith, and R. Andrews.** Diesel injection: laser light sheet illumination of the development of cavitation in orifices. *IMechE Conference on Fuel Injection Systems for IC Engines, London*, 1998.

8 **Chaves, H., M. Knapp, A. Kubitzek, and F. Obermeier.** Experimental Study of Cavitation in the Nozzle Hole of Diesel Injectors Using Transparent Nozzles. *SAE Technical Paper 950290*, 1995 .

9 **Badock, C., R. Wirth, A. Fath, and A. Leipertz.** Investigation of cavitation in real size diesel injection nozzles. *International Journal of Heat and Fluid Flow*, 1999, **20**, 538-544.

10 **Blessing, M., G. König, C. Krüger, U. Michels, and S. V.** Analysis of Flow and Cavitation Phenomena in Diesel Injection Nozzles and its Effect on Spray and Mixture Formation. *SAE Technical Paper 2003-01-1358*, 2003 .

11 **Chaves, H. and F. Obermeier.** Correlation between Light Absorption Signals of Cavitating Nozzle Flow within and outside of the Hole of a Transparent Diesel Injection Nozzle. In 14th ILASS-Europe, Manchester, UK, July 6-8, 1998

12 **LeCoz, J. F. and T. Baritaud.** Application of Laser Induced Fluorescence for Measuring the Thickness of Liquid Films on Transparent Wall. In 7th International Symposium on Applications of Laser Techniques to Fluid Mechanics, Lisbon, Portugal. 1994.

13 **Roth, H., M. Gavaises, and C. Arcoumanis.** Cavitation Initiation, Its Development and Link with Flow Turbulence in Diesel Injector Nozzles. *SAE Technical Paper 2002-01-0214*, 2002.

14 **Gavaises, M., A. Andriotis, D. Papoulias, N. Mitroglou, and A. Theodorakakos.** Characterization of string cavitation in large-scale Diesel nozzles with tapered holes. *Physics of Fluids*, 2009, **21**, 052107.

15 **Mitroglou, N., J. M. Nouri, and C. Arcoumanis.** In-nozzle cavitating flow and ambient temperature effects in high-pressure multi-hole gasoline sprays. *IMechE Conference on Fuel Injection Systems for IC Engines, London* , 2012, London, 13-14 May, 2009.

16 **Nouri, J. M., N. Mitroglou, Y. Yan, and C. Arcoumanis.** Internal Flow and Cavitation in a Multi-Hole Injector for Gasoline Direct-Injection Engines. *SAE Technical paper 2007-01-1405*, 2007.

17 **Andriotis, A., M. Gavaises, and C. Arcoumanis.** Vortex flow and Cavitation in Diesel Injector Nozzles. *Journal of Fluid Mechanics*, 2008, **10**, 195-215.

18 **Hsiao, C. T. and G. L. Chahine.** Numerical study of cavitation inception due to vortex/vortex interaction in a ducted propulsor. *Journal of Ship Research*, 2008, **52**, 114-123.

19 **Arndt, R. E. A.** Cavitation in fluid machinery and hydraulic structures. *Annual Review of Fluid Mechanics*, 1981, **13**, 273-326.

20 **Boulon, O., M. Callenaere, J. P. Franc, and J. M. Michel.** An experimental insight into the effect of confinement on tip vortex cavitation of an elliptical hydrofoil. *Journal of Fluid Mechanics*, 1999, **390**, 1-23.

21 **Hsiao, C. T. and L. L. Pauley.** Numerical study of the steady-state tip vortex flow over a finite-span hydrofoil. *Journal of Fluids Engineering*, 1998, **120**, 345.

22 **Gavaises, M., D. Papoulias, A. Andriotis, E. Giannadakis, and A. Theodorakakos.** Link Between Cavitation Development and Erosion Damage in Diesel Injector Nozzles. SAE Technical Paper 2007-01-0246, 2007.

23 **Andriotis, A. and M. Gavaises.** Influence of vortex flow and cavitation on near-nozzle diesel spray dispersion angle. *Atomization and Sprays*, 2009, **19**, 247.

24 **Mitroglou, N., M. Gavaises, J. M. Nouri, and C. Arcoumanis.** Cavitation inside enlarged and real-size fully transparent injector nozzles and its effect on near nozzle spray formation. In Cossali, G.E.; Tonini, S. (Eds.), Proceedings of the DIPSI Workshop 2011., pp. 33-45.

25 **Giannadakis, E., M. Gavaises, and C. Arcoumanis.** Modelling of cavitation in diesel injector nozzles. *Journal of Fluid Mechanics*, 2008, **616**, 153-193.

26 **Shih, T., W. W. Liou, A. Shabbir, Z. Yang, and J. Zhu.** A New Eddy-Viscosity Model for High Reynolds Number Turbulent Flows - Model Development and Validation. *Computers in Fluids*, 1995, **24**, 227-238.

27 **Kader, B.** Temperature and Concentration Profiles in Fully Turbulent Boundary Layers. *Int. J. Heat Mass Transfer*, 1981, **24**, 1541-1544.

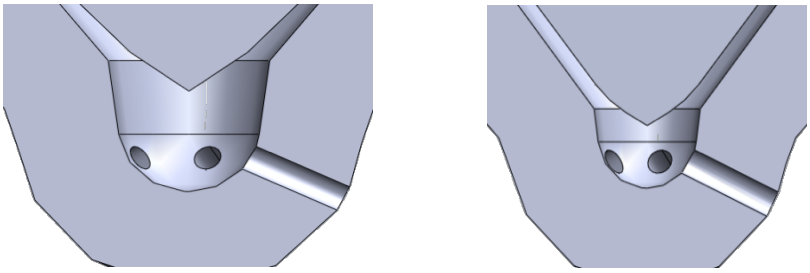

a b

Figure 1: Schematic of the investigated nozzles a. large sac volume nozzle geometry and b. small sac volume nozzle geometry.

Table 1: Experimental conditions for the 5-hole nozzles

	Reynolds Number	Cavitation Number	5-hole	Sac height	Sac volume
Large Sac volume	20,000 – 54,000	5 – 21	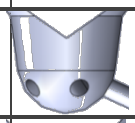	11.15mm	1035mm^3
Small Sac volume	12,000 – 44,000	5 – 21	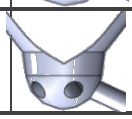	6.5mm	340mm^3

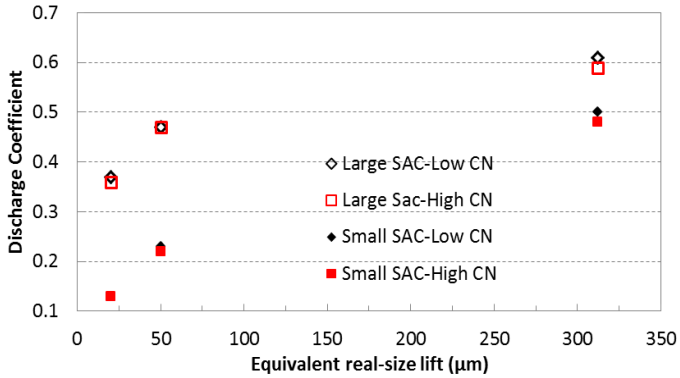

Figure 2: Measured discharge coefficient of the two nozzles for all tested operating conditions.

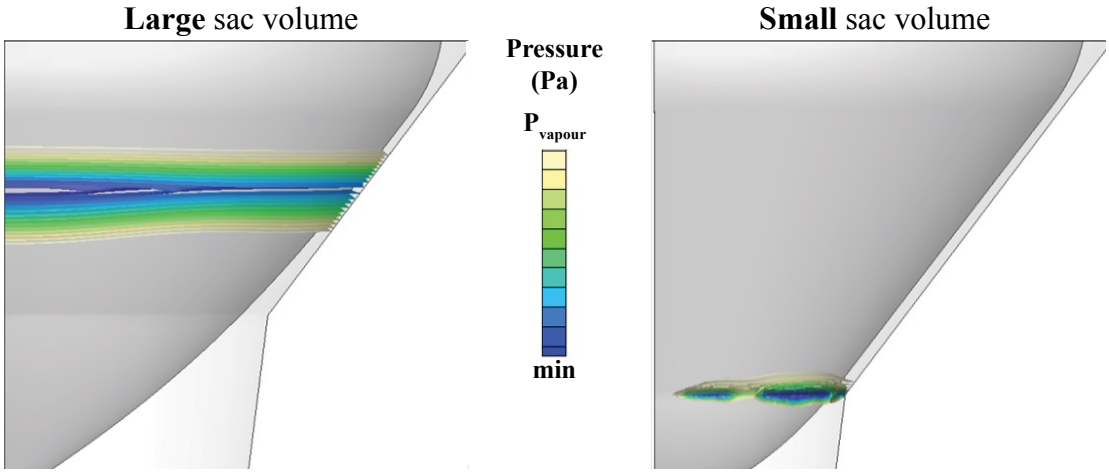

Figure 3: Predicted pressure distribution along the needle valve seat at 20µm lift, P_{inj} = 7.5 bar, P_{back} = 0.98 bar, CN = 7. The selected colour scale reveals the areas with pressure below the threshold value of cavitation inception.

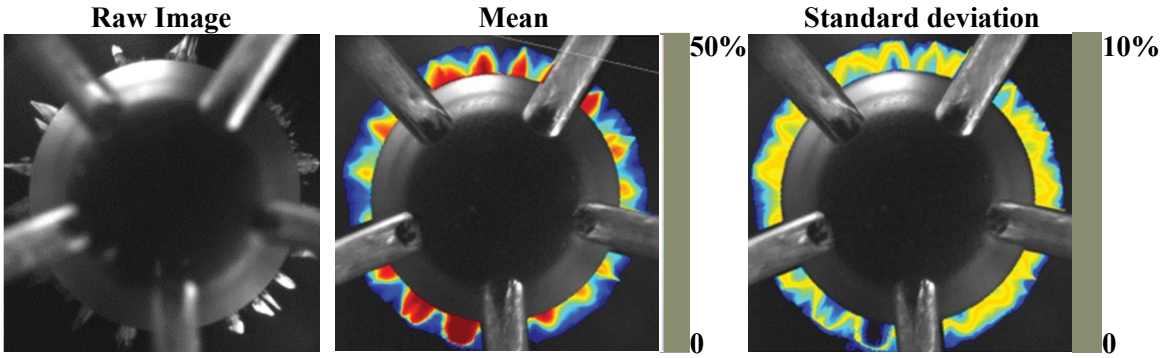

Figure 4: Bottom view images of cavitation in the needle seat area of the large sac volume nozzle. a. Representative raw image b. mean image obtained from 10000 images acquired over 0.5s duration and c. standard deviation. (20µm equivalent real-size lift, CN = 7).

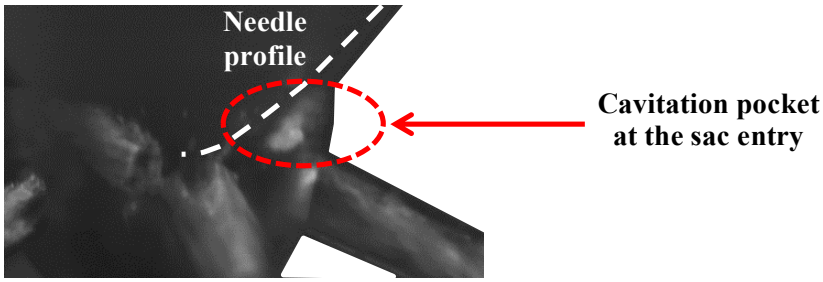

Figure 5: Representative image of the observed cavitation pockets downstream the needle seat and at the sac volume entry region, for the small sac volume nozzle at 20µm equivalent real-size lift, CN = 7.

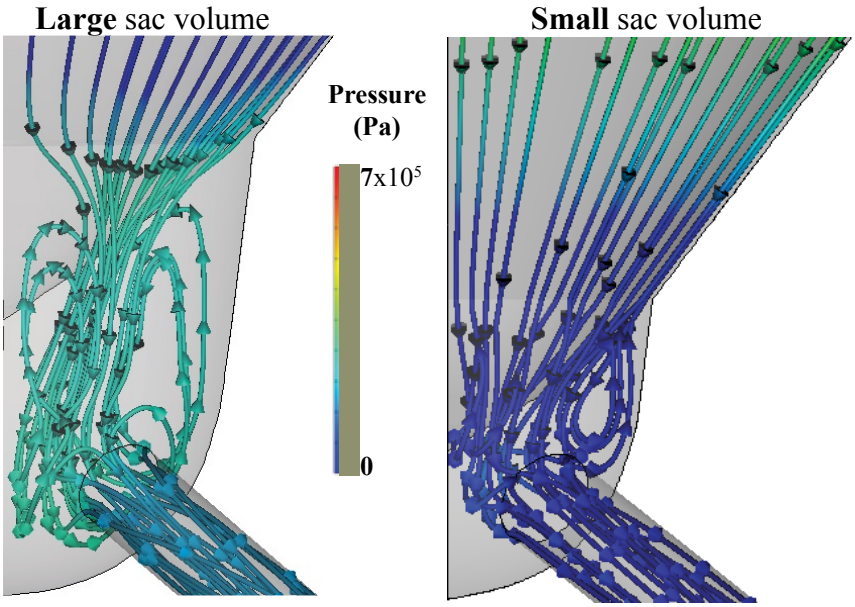

Figure 6: Predicted flow streamlines inside the sac volume of both nozzles at 20µm equivalent real-size lift, CN = 7 (P_{in} = 7.5 bar, P_{back} = 0.98 bar).

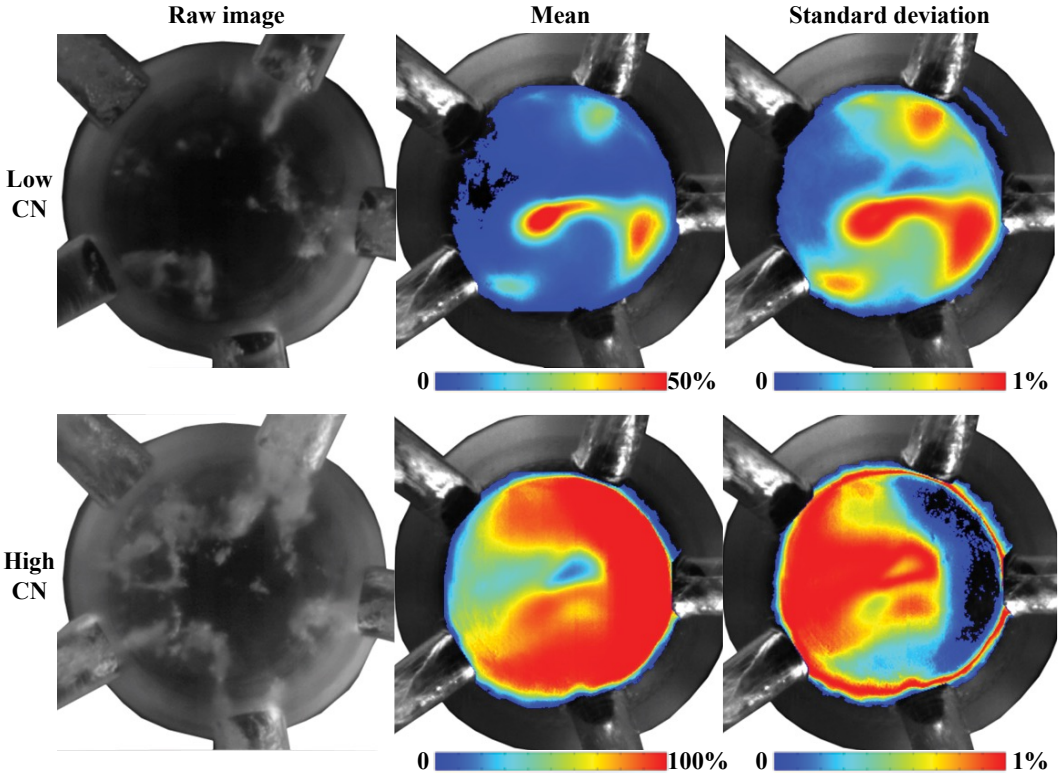

Figure 7: String cavitation investigations inside the small sac volume nozzle at 20µm equivalent real size needle lift, Low CN = 7 and high CN = 19.

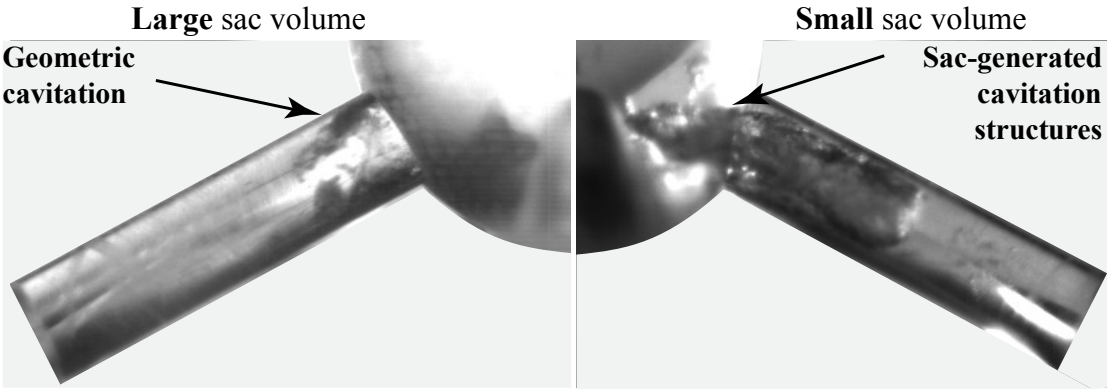

Figure 8: Comparison of hole cavitation structures between the large and small sac volume nozzles at 20µm equivalent needle lift of the real size injector (CN = 7).

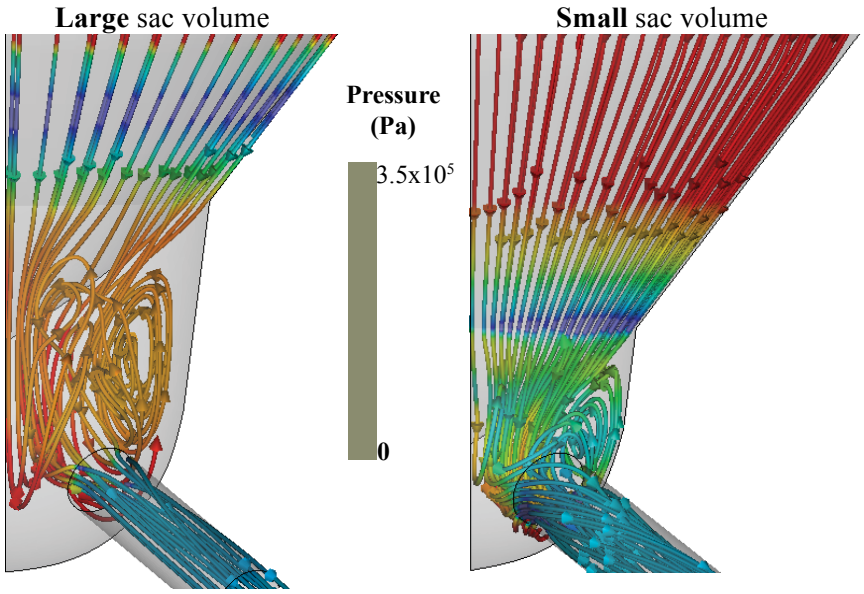

Figure 9: Predicted flow streamlines inside both nozzles at 50µm equivalent real-size needle lift, CN = 11.

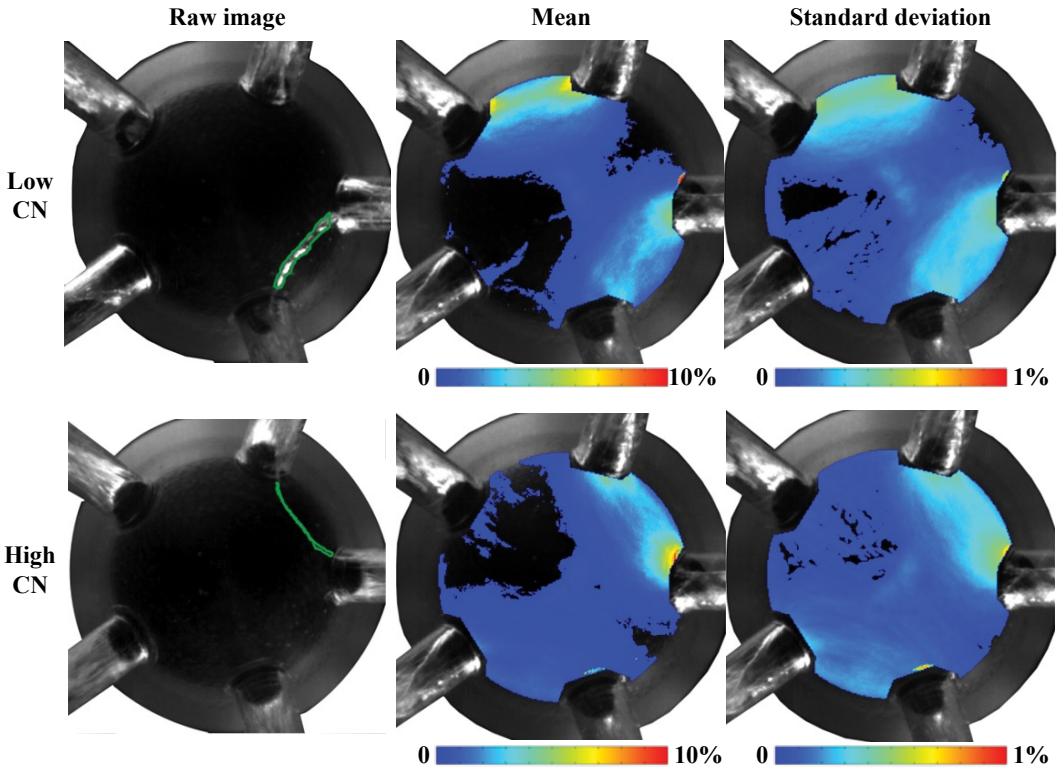

Figure 10: String cavitation investigations inside the large sac volume nozzle at 50µm equivalent real-size needle lift, low CN = 6 and high CN = 18.

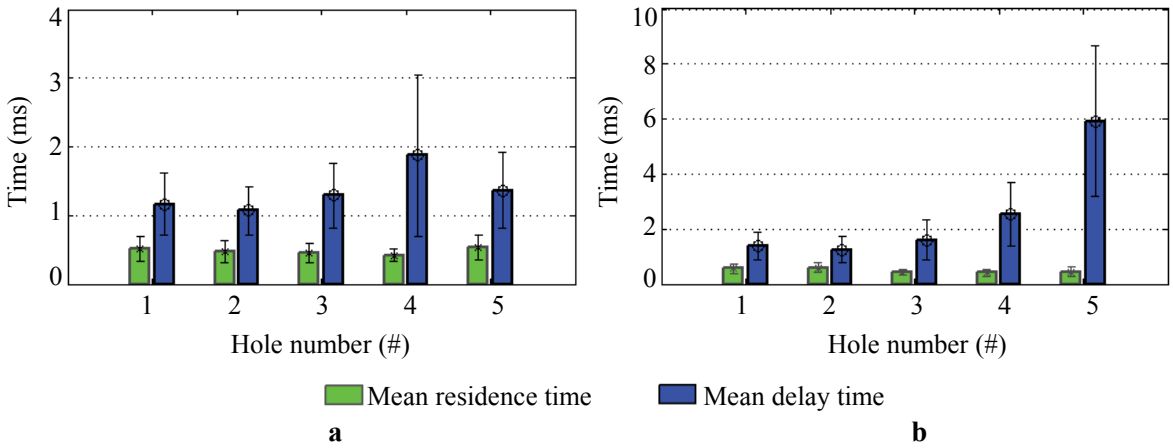

a **b**

Figure 11: Mean residence and delay times of string cavitation appearance per injection hole inside the large sac volume nozzle with the measured standard deviation plotted as error bar. a. Low CN = 6, b. High CN = 18.

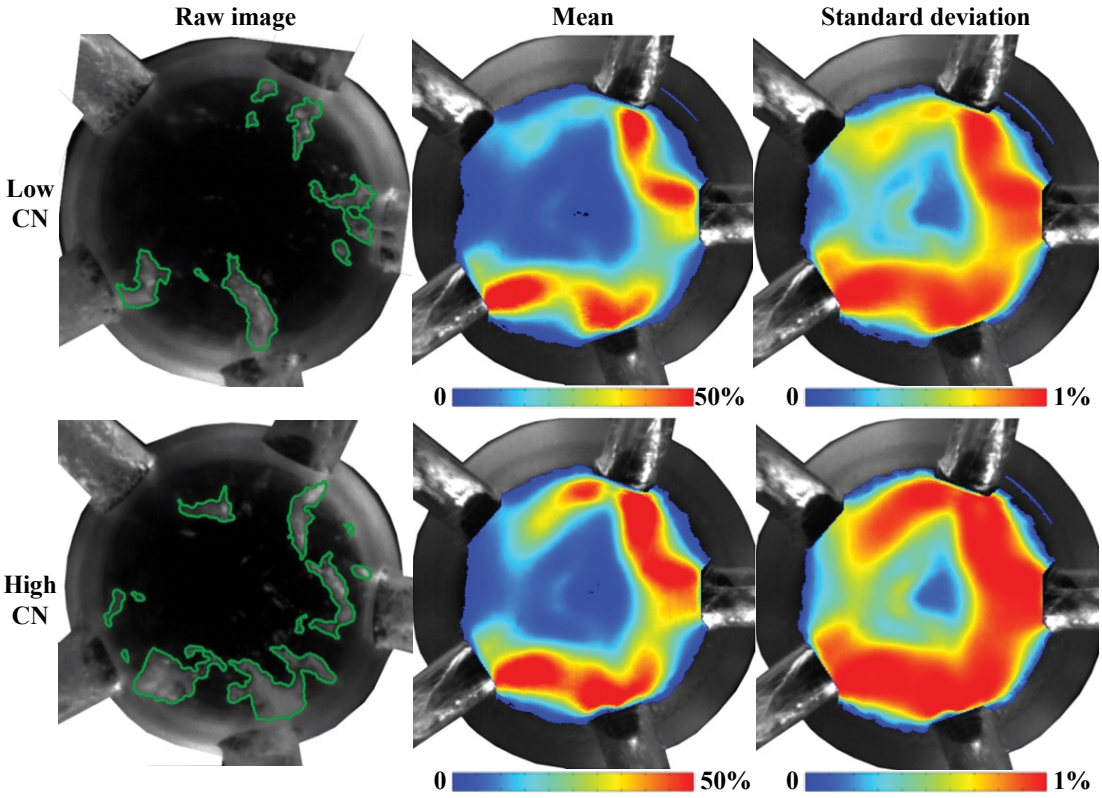

Figure 12: String cavitation investigations inside the small sac volume nozzle at 50µm equivalent real-size needle lift, low CN = 7, high CN = 18.

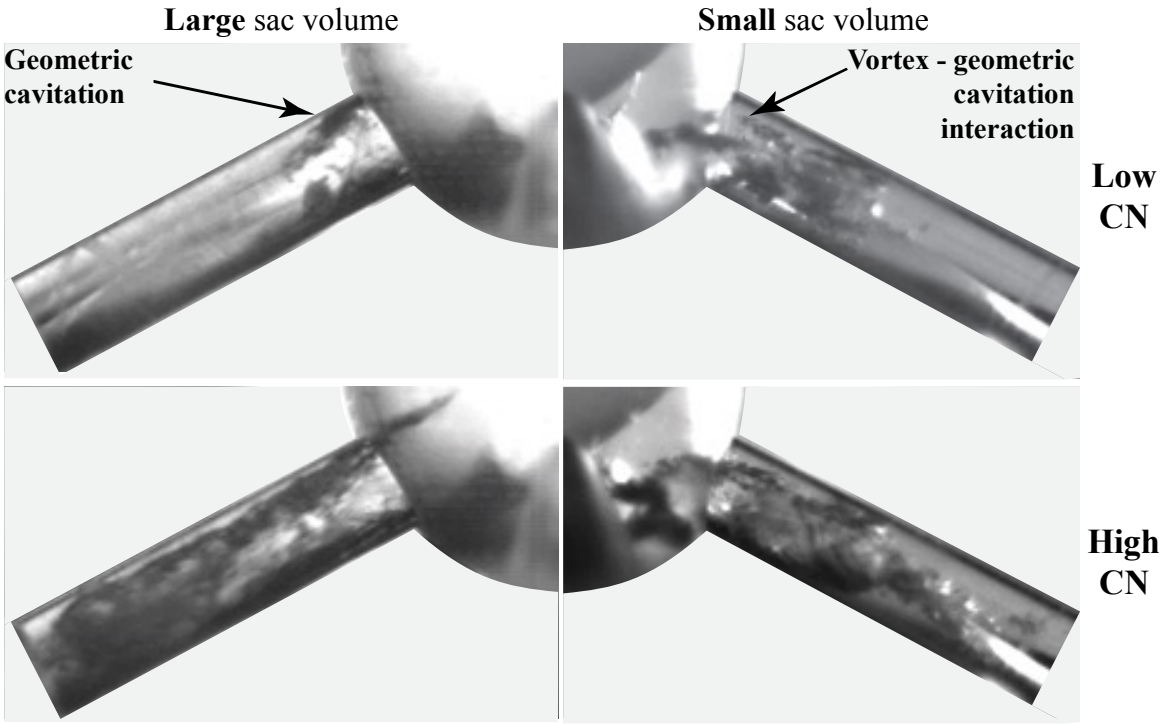

Figure 13: Comparison of hole cavitation structures between the large and small sac volume nozzles at 50µm equivalent real-size. Large sac volume: low CN = 6 and high CN = 18. Small sac volume: low CN = 7, high CN = 18.

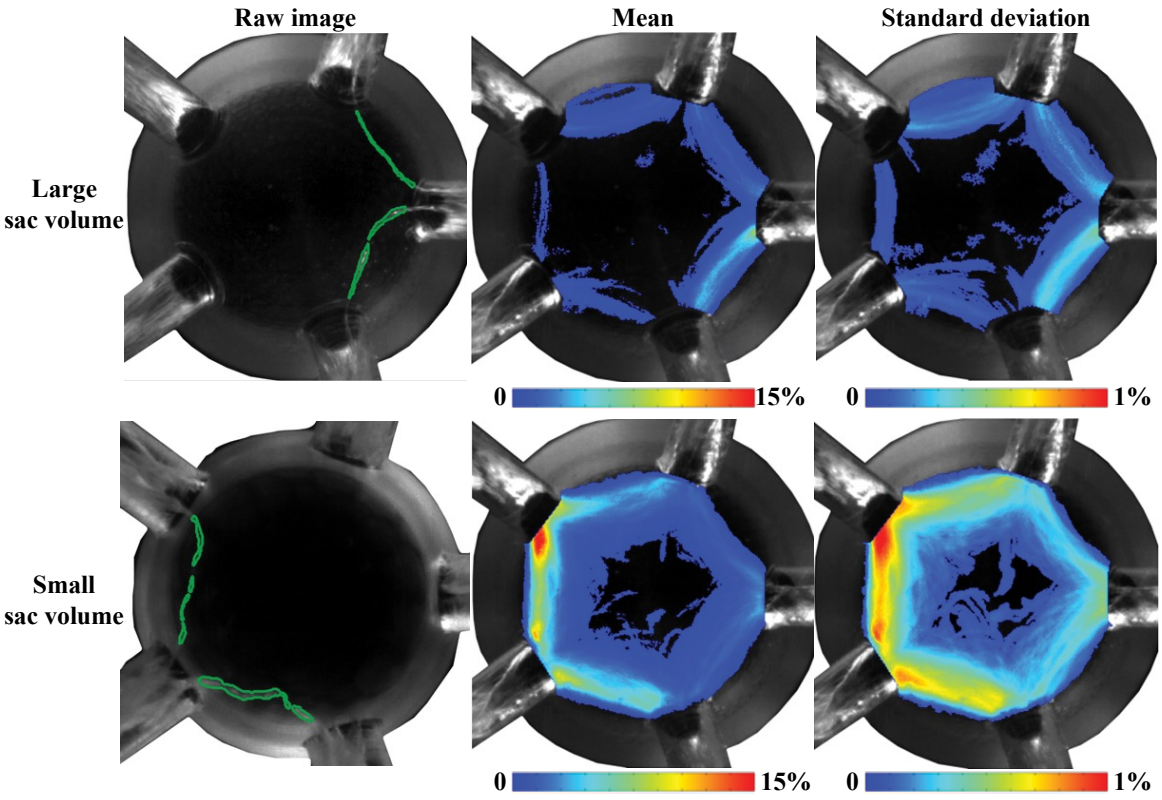

Figure 14: String cavitation investigations inside the sac volume of both nozzles investigated at full needle lift, CN = 13.

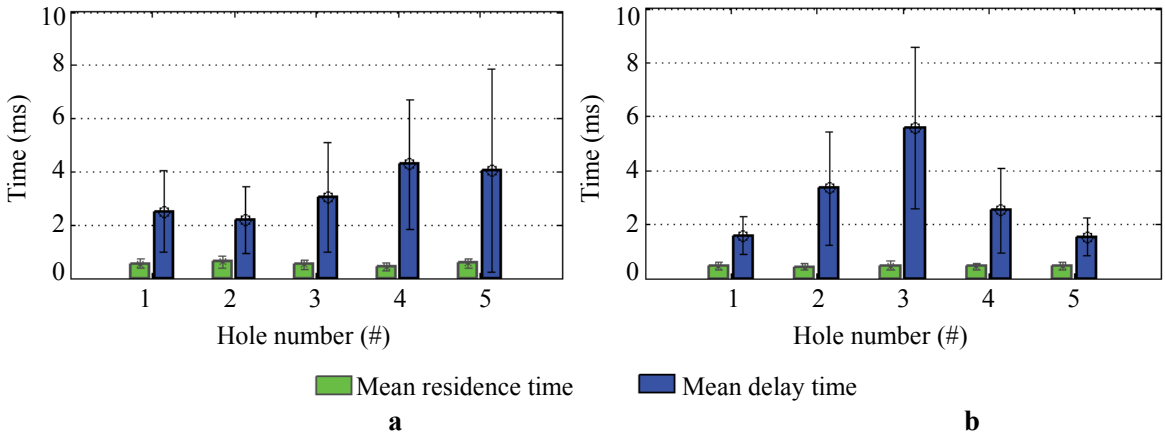

Figure 15: Mean residence and delay times of string cavitation appearance per injection hole; measured standard deviation is plotted as error bars. a. Large sac volume, CN = 13 and b. Small sac volume, CN = 13.

Large sac volume

Small sac volume

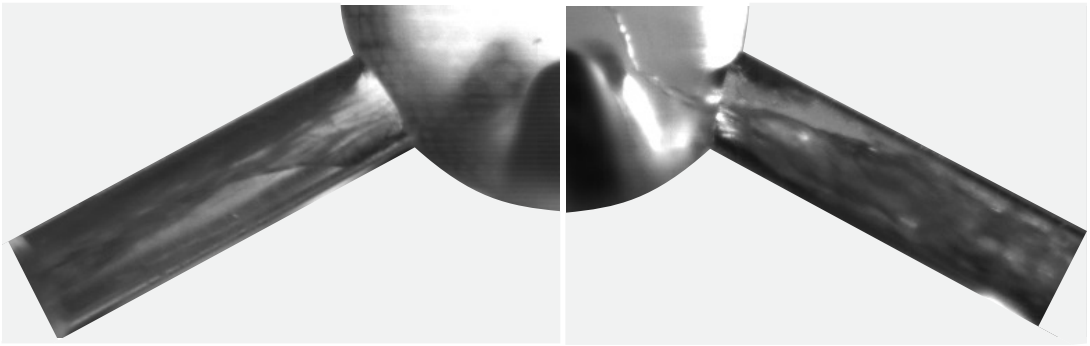

Figure 16: Representative raw images of cavitation structures inside injection holes of the large and the small sac volume nozzles at full needle valve lift and CN = 13.